51st AIAA Aerospace Sciences Meeting including the New Horizons Forum and Aerospace Exposition
07 - 10 January 2013, Grapevine (Dallas/Ft. Worth Region), Texas

AIAA 2013-0626

# A MEMS Floating Element with Bump Shear Stress Sensor Array on a Chip

Zhengxin Zhao[1], Minchul Shin[2] and Robert D. White[3]
*Mechanical Engineering, Tufts University, Medford, MA 02155*

*and*

Judith Gallman[4]
*Spirit Aerosystems, Wichita, KS 67210*



**A MEMS floating element shear stress sensor with bumps has been designed in a 1cm by 1cm chip. The array consists of 256 individual floating elements (16 groups), and each element supports 35 bumps on the top surface. The sensor was fabricated using four layers of surface micromachining including copper & nickel electroplating. The chip is packaged in a ceramic package and flush mounted into a flow channel. Experimental characterization indicates: a) a static sensitivity of 0.6 fF/Pa in the laminar flow range of Reynolds number = 0~1500; b) a linear range up to 13 Pa shear stress; c) a resolution of 44 mPa/rtHz; d) a first mode resonant frequency of 18 kHz.**

## I. Introduction

Techniques for skin friction and shear stress measurement have been described as early as 1954 [1-4], however, they are inadequate for some applications due to their poor spatial and temporal resolution. In the last two decades, MEMS-based shear stress sensors have emerged as a possible scheme for wall shear stress measurement, and have been developed by the various groups [5-9].

The previous MEMS-based sensors to appear in the literature have two common features: 1) all MEMS-based floating element shear stress sensor were produced as individual floating elements fabricated on a silicon wafer and calibrated only up to 1~2 Pa; 2) A majority of MEMS-based sensors besides floating element also have been tested only up to 1~2 Pa [6,8,9]. However, this paper is focusing on high wall shear stress characterization. The modification of the floating element to include surface bumps is intended to improve the sensitivity, but may also increase the maximum detectable shear stress. Secondly, this paper introduces a shear stress sensor array-on-a-chip, in which we array the individual sensing elements into a group, and combine several groups in parallel on a chip to create an array-in-an-array sensor topology. Therefore, one chip consists of 4 by 4 groups, each of which has 4 by 4 elements as one signal output. The spatial resolution of the array-on-a-chip is on the order of a millimeter. The local shear stress or average shear of a single chip is capable of being detected simultaneously and conveniently. Another benefit of an array sensor is to avoid the problem of defects in fabrication on single element destroying the functionality of the whole sensor chip.

Additionally, two kinds of electronics have provided more options of sensor calibration: analog or digital, voltage or capacitance. Finally, the sensor in this paper was built on the glass substrate instead of a silicon wafer in order to reduce parasitic capacitance as well as the driven current or voltage to the sensor.

## II. Design

The design of this sensor has many similarities with MEMS floating element shear stress sensors described in the past. As described in [7], one floating element has a movable center shuttle which experiences shear stress from the

[1] Research Assistant, Mechanical Engineering, 200 College Ave, Medford, MA 02155, AIAA Member
[2] Research Assistant, Mechanical Engineering, 200 College Ave, Medford, MA 02155
[3] Associate Professor, Mechanical Engineering, 200 College Ave, Medford, MA 02155, Senior AIAA Member
[4] Associate Technical Fellow, Spirit Aerosystems, 3801 S. Oliver St., Kichita, KS, 67210, Senior AIAA Member

flow, two sets of comb finger for driving or sensing the motion of shuttle, and a series of folded beam to act as a spring and support the shuttle. The sensor stiffness in the out-of-plane and lateral in-plane directions are [5]:

$$K_z = 2Ew\left(\frac{t}{L}\right)^3 \tag{1}$$

$$K_y = 2Et\left(\frac{w}{L}\right)^3 \tag{2}$$

where $E$ is young's modulus, $w$, $t$, and $L$ are the width, thickness, and length of beam, respectively. The change of capacitance of the floating element at DC is proportional to the shear stress if ignoring the fringe effects on the combs and out-of-plane motion (only in-plane motion) [9]:

$$S_1 = \frac{\Delta C}{\tau} = \frac{N\varepsilon L^3 A_m}{Edw^3} \tag{3}$$

where $N$ is the number of fingers, $\varepsilon$ is absolute permittivity of air, and $A_m$ is the surface area of shuttle. In order to minimize the out-of-plane motion, the thickness (or the ratio of $w/t$) should be as high as possible, and so the floating element is much more flexible in-plane than out-of-plane, as shown in Eq. (1-2). However, the thickness to width ratio is limited by the fabrication process capabilities.

The design of one floating element with 35 dark bumps is shown in **Figure 1 a),** and more critical dimensions of the bump-floating element are given in **Table 1**. **Figure 1 b)** shows the layout of 4 by 4 groups in one chip and 4 by 4 elements on one group. The bumps on the surface of the sensor should have an impact on the sensitivity of Eq.(3) since more lateral force is expected due to the interaction of the flow with the rough surface. Comsol Multiphysics was used to predict the force generated on the half of a symmetric single bump. The steady, fluid dynamic simulation result is shown in **Figure 2**. In this simulation, a Poiseuille profile identical to that used in our laminar flow cell is introduced from the side, and the steady flow around the bump is calculated using N-S with an incompressible, viscous Newtonian fluid model.

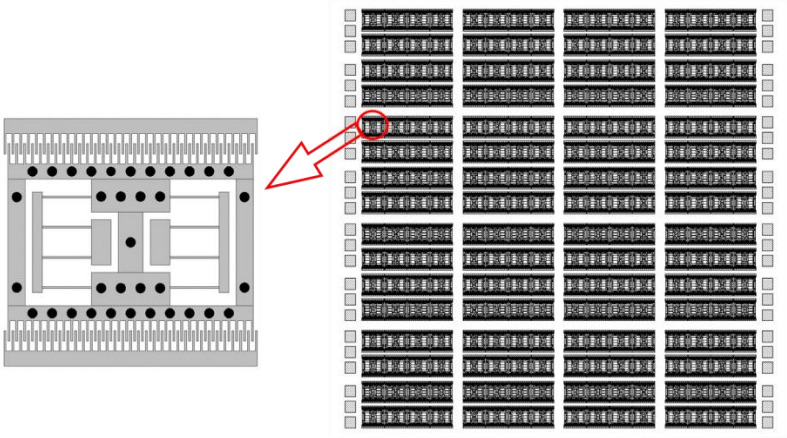

a) b)

**Figure 1. A schematic of a) one floating element with 35 bumps, b) 256 element array on a chip.**

The force on the half bump is $F = 8\ nN$ as given by surface integration of both pressure and shear stress in COMSOL. Thus the total force due to 35 bumps on one element is $F_2 = 35 \cdot 2 \cdot F = 0.58 \cdot \mu N$. For the same conditions, the wall shear force on the non-bump-element simply due to shear stress at the surface is $F_1 = 0.45\ \mu N$. Thus, the sensitivity of bump-element can be estimated as

$$S_2 = S_1 \cdot \frac{F_2 + F_1}{F_1} = \frac{2.3N\varepsilon L^3 A_m}{Edw^3} \tag{4}$$

**Table 1. Designed and Manufactured dimension of the floating element with bump**

| Critical Dimension | Designed | Manufactured |
|---|---|---|
| Finger Gap d (um) | 4 | 4.8 |
| Thickness of folded beam t (um) | 8 | 8.8 |
| Width of folded beam w (um) | 4 | 5.1 |
| Height of bump h (um) | 12 | 12 |
| Diameter of bump D (um) | 20 | 25 |
| Length of folded beam L (um) | 100 | 100 |
| Number of comb teeth per element N | 64 | 64 |
| Shuttle top area $A_m$ ($mm^2$) | 0.083 | 0.083 |
| Modulus of Nickel (GPa) | 200 | 200 |
| Predicted sensitivity $S_2$ per group (aF/Pa) | 34 | 14 |
| Measured sensitivity per group (aF/Pa) | | 64 |

This assumes that as flow increases, the ratio of force for flow around the bumps to force on the flat plate remains approximately the same. This is expected to be true for low flow rates where the Navier Stokes equations are close to linear. However, at higher flow rates a separate flow calculation would need to be done at each flow rate, and, once turbulent flow was established, a more sophisticated model would be required. The purpose of this calculation is primarily to provide a first estimate of the increase in sensitivity expected in the laminar flow test setup.

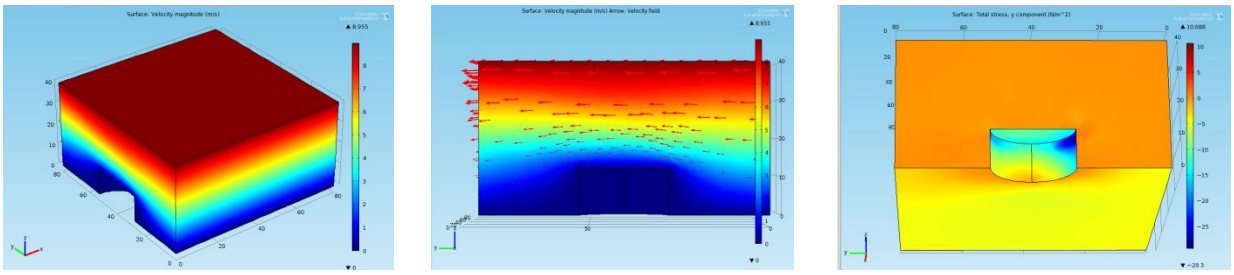

a) b) c)

**Figure 2. COMSOL model: a) 3D velocity profile of laminar duct flow, b) 2D velocity profile along the bump, c) Pressure distribution around the bump.**

## III. Fabrication and Package

The sensor was fabricated using a four-mask nickel surface micromachining in the Tufts Micro/Nano Fab, as shown in **Figure 3**. The process starts with a soda lime glass wafer of 550 μm thickness. 75 nm/250 nm thick Cr/Au interconnects, followed by another thin seed layer Ti/Cu (30nm/300nm) were sputter deposited and patterned by liftoff using a two layer liftoff resist process. Next, a photoresist layer was photolithographycially patterned to form anchor regions to the substrate. A 5 μm sacrificial layer of copper was electroplated on the top of seed layer to cover the entire substrate except the anchor regions. The 9 μm height floating element and 12 μm height bump layers were electroplated in two steps using a commercial nickel sulfamate plating solution. The pattern was established using a thick photoresist (AZ9260). Care was taken to minimize the surface roughness by controlling the plating current and brightener percentage as well as agitating and filtering the plating solution. Then, a protective photoresist layer was spun on for dicing. Finally, the sacrificial copper layer was etched away in a mixture of 1 part Acetic Acid to 1 part 30% Hydrogen Peroxide to 18 parts DI water for 24 hours and then chip is rinsed in water, isopropanol, and methanol, and allowed to air dry in a dry box that has been flooded with clean dry air with a low relative humidity. The released structure of the comb finger details, a bump detial, and a micrograph of the full element are shown in **Figure 4**. The design and manufactured geometry for the sesnor characterized in the paper as well as the predicted sensitivity is given in **Table 1**.

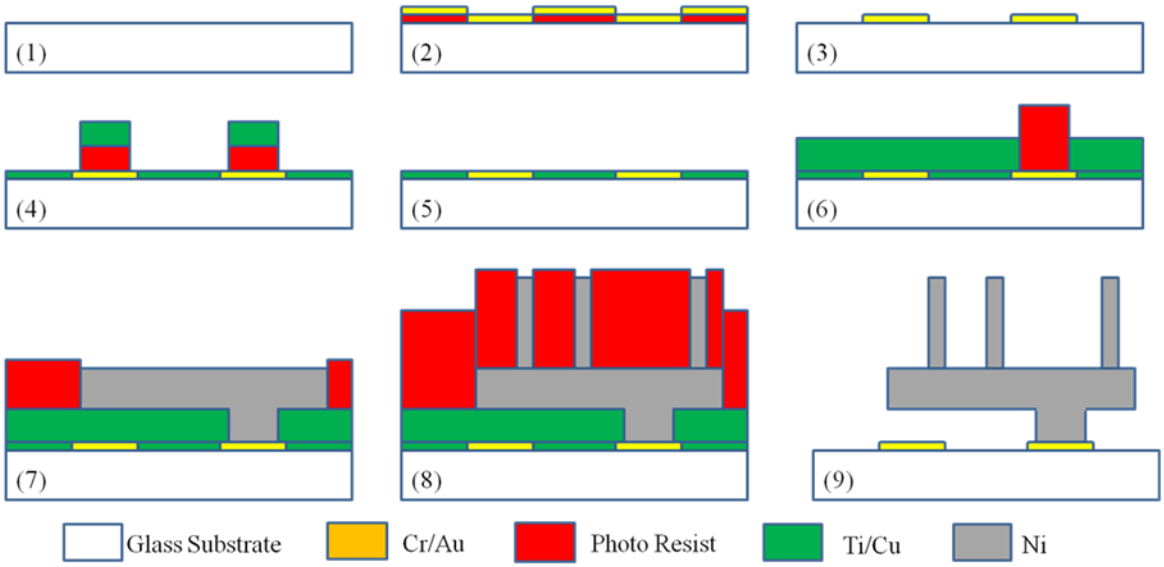


**Figure 3. A Schematic of fabrication process flow**

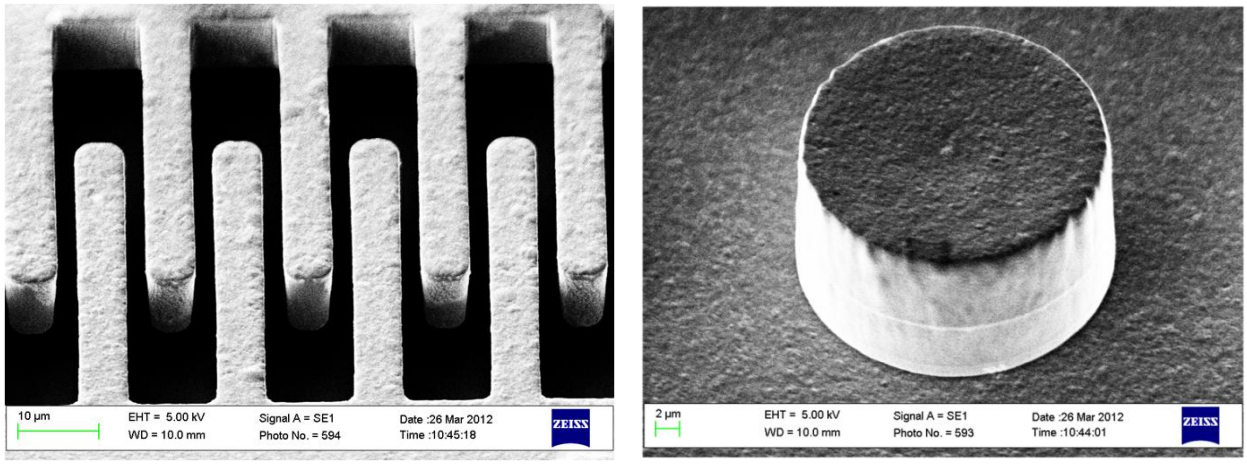


a) b)

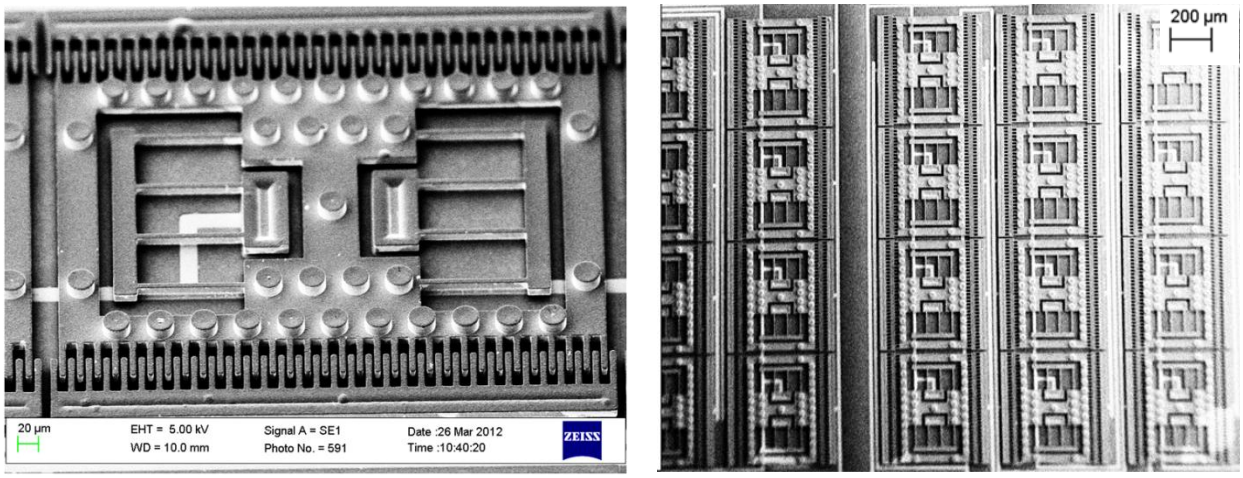


c) d)

**Figure 4. SEM Images of a) Comb finger, b) One bump, c) One element, d) One group**

The chip is next packaged in a 4 cm by 4 cm ceramic pin grid array hybrid package (CPGA). First, the CPGA cavity is partially filled with potting epoxy [Namics Chipcoat G8345-6] which is cured. The epoxy is then CNC milled to the appropriate height, including a small square pocket to center and align the chip. The chip is mounted into the pocket with a thin epoxy film. The package is ball bonded to the chip using 25 micrometer diameter gold wire. Finally, the wirebonds are potted in epoxy, which is allowed to settle and cure, with multiple layers being applied until a flat surface is achieved around the chip and package. Using this method, it is possible to create a flat surface with a total maximum topology from the ceramic surface, onto the epoxy, over the wirebonds and onto the chip of approximately 100 micrometers. **Figure 5** shows a photograph of a packaged chip.

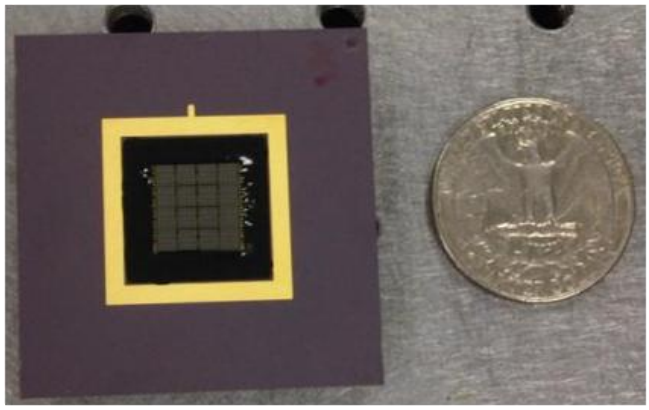

**Figure 5. Photograph of a packaged array chip.**

## IV. Experiment Setup: Flowcell and Electronics

The flowcell used in this paper is similar with previous work presented in the literature [5, 9]. The flow channel illustrated in **Figure 6** was created by milling a thin rectangular slot into an aluminum plate, and assembling this with a flat bottom plate flush mounted to the chip. The slot is shallow and wide in order to get very high aspect ratio (~70) flow channel, reduce the entrance length (~0.1 m), obtain shear stress as high as possible within the laminar region (13 Pa when Re ~ 2000), fast flow speed (0.15 Mach when Re ~2000). The inlet air is regulated by a digital flow controller (Omega FMA3812), which is controlling the volume flow rate from 0 to 40 CFH (cubic feet per hour). The outlet flow exits to atmosphere. Five pressure taps are used to characterize the pressure gradient, from which it is possible to infer the wall shear stress. The Reynolds number exceeds 2300 when the flow rate is over 40 CFH, and thus the maximum achievable shear stress for laminar flow is limited to 13 Pa. For high flow, the shear stress, as estimated by pressure gradient, does not follow the linear line as in the low speed region, as shown in **Figure 7**. This implies that the flow is transitioning to turbulence at flow rates above 40 CFH, as expected from the Reynolds number calculations.

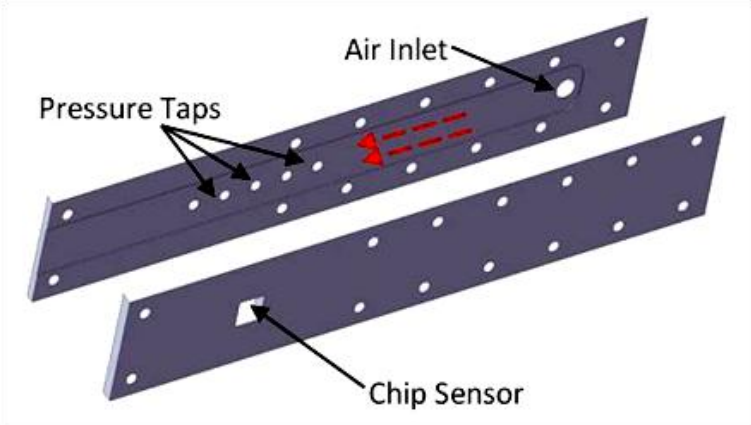


**Figure 6. A schematic of a disassembled Flowcell.**

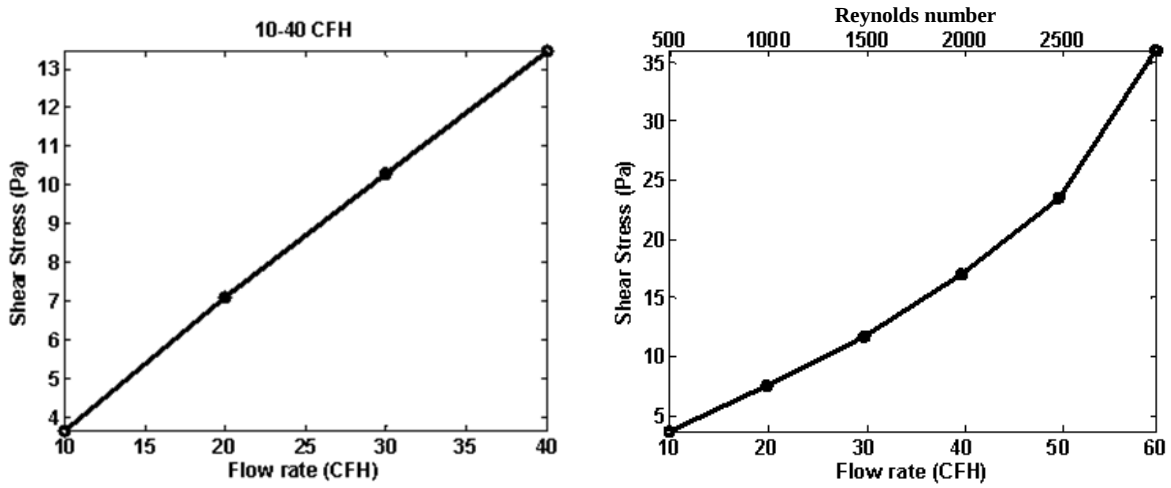


a) b)

**Figure 7. Shear stress in the laminar flow cell calculated from the measured pressure gradient. a) Shear stress vs. flow rate at low flow rates, b) Shear stress vs. flow rate at higher flow rates.**

We are presenting two kinds of electronics to calibrate the sensor: Analog Voltage and Digital Capacitance electronics. For the analog electronics, the core part of the electronics is a MS3110 Universal Capacitive Readout Chip from Irvine Sensors, which includes an on-chip variable capacitive DAC for initial differential adjustment of dual channels, a low pass filter of programmable cutoff frequency from 500 Hz to 8 kHz, and requires a 5V DC driven voltage. Dual channels of the MS3110 are connected to the top and bottom electrodes of the floating element, respectively, so this differential measurement has an advantage to partially cancel out the mutual temperature, humidity or other environment noise that may cause common mode capacitance change. The transfer function of the MS3110 chip is provided by the manufacturer,

$$V_0 = \text{Gain} \cdot [(\text{CS1IN} + \text{CS1}) - (\text{CS2IN} + \text{CS2})]/C_f + \text{DC} \tag{5}$$

where the Gain, CS2, CS1, $C_f$, DC are all adjustable parameters of MS3110, and CS1IN and CS2IN represent the two capacitors of the sensor. Therefore, the output voltage $V_0$ will be proportional to the difference between top and bottom capacitance output. As a second solution, the AD7747 chip from Analog Devices, which is a 24-Bit capacitance-to-digital converter, has been used for the digital measurement. This measurement is also differential.

## V. Calibration Results

The MEMS shear sensor has been flush mounted and tested in the flow channel as described in the previous section. **Figure 8** indicates calibration result of the floating element with bumps array sensor for 10 groups on the MS3110 analog voltage electronics and 9 groups on AD7747 digital capacitance electronics. Comparison between two schemes of electronics has shown the digital electronics performs with lower noise and higher resolution, achieving 44 mPa/rtHz. Nonlinearity is 0.6% at a shear stress of 12.7 Pa. The sensitivity 0.58 fF/Pa for 9 groups shows 1) the sensitivity of one group is 64 aF/Pa, which is 4.6 times higher than the prediction based on manufactured dimensions shown in Table 1; and 2) a sensitivity of whole chip with 16 groups will be as high as 0.1 pF/Pa. The predicted sensitivity is on the same order as the measured sensitivity, but the higher measured sensitivity suggests that additional forcing is present, perhaps from flow around the sides and bottom of the floating element structures, which has not yet been considered in the model **Figure 9** shows the experimental repeatability and consistent sensitivity. Low frequency drifting is observed, but reduces over time. After settling to steady state, the average of drift is approximately 0.02 mV/min, which equates to 0.1 Pa/min.

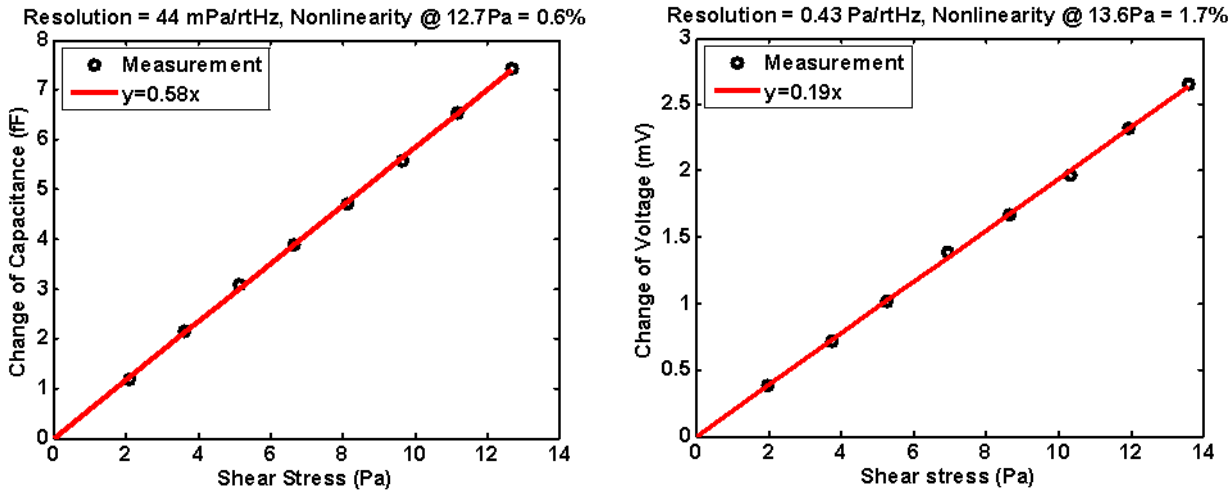


a) b)

**Figure 9. Calibration result using a) MS3110 and b) AD7747**

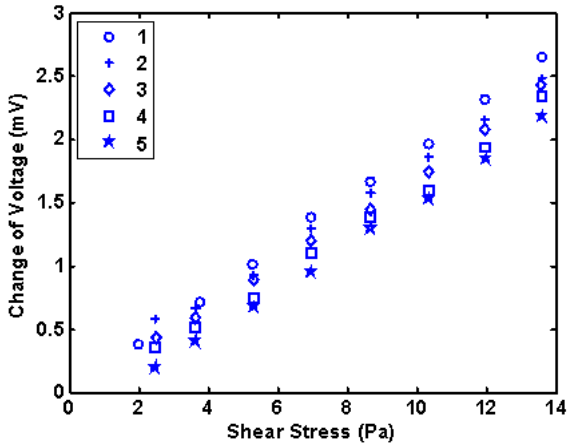


**Figure 8. Repeatability of sensitivity for 5 calibration runs. An offset drift is observed, but sensitivity remains consistent.**

## VI. Conclusions

The unique topology of array-based shear stress sensor of floating element was developed with the goal of achieving both small (~0.5 mm) and large (~10 mm) spatial resolution simultaneously. A 1 cm square sensor chip with 5 μm air separation, 8.8 μm thick floating element and 12 μm high bumps has been fabricated, wirebonding with the CPGA package, and measured in the laminar flow measurement. The differential measurement using an AD7747 capacitance to digital chip demonstrates a detectable wall shear stress range up to 13 Pa with less than 1% nonlinearity; maximum achievable shear stress was limited by the testing setup, not the sensor. The calibration of a chip with 9 active groups shows a sensitivity of 0.6 fF/Pa at a noise level of 44 mPa/rtHz, thereby the dynamic range is greater than 50 dB/rtHz. A DC voltage drift is observed during operation. The drifting coefficient saturates at approximately 0.1 Pa/min. An effort to improve the yield (10 out of 16 is best so far) will be undertaken in future work, as well as additional analysis of the microscale flow, and investigation of possible sources of error such as pressure gradient effects and misalignment.

## References


1. J. H. Preston, "*The determination of turbulent skin friction by means of Pitot tubes*" Journal of the Royal Aeronautical Society,vol. 58, pp. 109–121, (1954).
2. M. R. Head and I. Rechenberg, "*The Preston tube as a means of measuring skin friction*" (1962).
3. M. R. Head and V. V. Ram, "*Simplified presentation of Prestontube calibration(Preston skin friction measuring tube calibration,presenting Patel analytic method simplification*" Aeronautical Quarterly, vol. 22, pp. 295-300, (1971)
4. K. G. Winter, "*An outline of the techniques available for the measurement of skin friction in turbulent boundary layers*" Progress in Aerospace Sciences, vol. 18, pp. 1-57, (1979).
5. M. A. Schmidt, R. T. Howe, S. D. Senturia, J. H. Haritonidis, and C. Mit, "*Design and calibration of a microfabricated floating-element shear-stress sensor*" IEEE Transactions on Electron Devices, vol. 35, (1988).
6. A. Padmanabhan, H. Goldberg, K. D. Breuer, and M. A. Schmidt, "*A wafer-bonded floating-element shear stress microsensor with optical position sensing by photodiodes*" Journal of Microelectromechanical Systems, vol. 5, (1996).
7. T. Pan, D. Hyman, M. Mehregany, E. Reshotko, and S. Garverick, "*Microfabricated shear stress sensors, part 1: design and fabrication*" AIAA Journal, vol. 37, (1999).
8. Chandrasekharan, V., Sells, J., Meloy, J., Arnold, D.P., Sheplak, M., "*A metal-on-silicon differential capacitive shear stress sensor*", in Solid-State Sensors, Actuators and Microsystems Conference, TRANSDUCERS, (2009).
9. Zhe J, Modi V, Farmer KR. "*A microfabricated wall shear-stress sensor with capacitive sensing"*. . Journal of Microelectromechanical Systems, vol. 14, pp. 167–175 (2005)